Atmos. Chem. Phys. Discuss., 12, 17397–17442, 2012
www.atmos-chem-phys-discuss.net/12/17397/2012/
doi:10.5194/acpd-12-17397-2012

Atmospheric Chemistry and Physics Discussions

Transport analysis and source attribution of seasonal and interannual variability of CO in the tropical upper troposphere and lower stratosphere

Junhua Liu[1], **J. A. Logan**[1], **L. T. Murray**[1], **H. C. Pumphrey**[2], **M. J. Schwartz**[3], **and I. A. Megretskaia**[1]

[1]School of Engineering and Applied Sciences, Harvard University, Cambridge, Massachusetts, USA
[2]School of Geosciences, The University of Edinburgh, Edinburgh, UK
[3]NASA Jet Propulsion Laboratory, Pasadena, California, USA

Received: 15 May 2012 – Accepted: 20 June 2012 – Published: 13 July 2012

Correspondence to: Junhua Liu (jliu@seas.harvard.edu)

Published by Copernicus Publications on behalf of the European Geosciences Union.

Abstract

We used the GEOS-Chem chemistry-transport model to investigate impacts of surface emissions and dynamical processes on the spatial and temporal patterns of CO observed by the Microwave Limb Sounder (MLS) in the upper troposphere and lower stratosphere (UTLS). Model simulations driven by GEOS-4 and GEOS-5 assimilated fields present many features of the seasonal and inter-annual variation of CO in the UTLS. Both model simulations and the MLS data show a transition from semi-annual variations in the UT to annual variations in the LS. Tagged CO simulations indicate that the semi-annual variation of CO in the UT is determined mainly by the temporal overlapping of surface biomass burning from different continents as well as the north-south shifts of deep convection. Both GEOS-4 and GEOS-5 have maximum upward transport in April and May with a minimum in July to September. The CO peaks from NH fires propagate faster to the LS than do those from SH fires. Thus the transition from a semi-annual to an annual cycle around 80 hPa is induced by a combination of the CO signal at the tropopause and the annual cycle of the Brewer-Dobson circulation. In GEOS-5, the shift to an annual cycle occurs at a lower altitude than in MLS CO, a result of inadequate upward transport. We deduce vertical velocities from MLS CO, and find that those in GEOS-4 agree well with them between 215 hPa and 125 hPa in boreal summer, fall and winter, while the velocities in GEOS-5 are too low in all seasons. The mean tropical vertical velocities from both models are lower than those inferred from MLS CO above 100 hPa in June to November, particularly in GEOS-5, with mean downward, rather than upward motion in boreal summer. Thus the models' CO maxima from SH burning are transported less effectively than those in MLS CO above 147 hPa and almost disappear by 100 hPa. The strongest peaks in the CO tape-recorder are in late 2004, 2006, and 2010, with the first two resulting from major fires in Indonesia and the last from severe burning in South America, all associated with intense droughts.

ACPD

12, 17397–17442, 2012

1 Introduction

It is well known that air enters the stratosphere in the tropics, driven by the adiabatic upwelling of the Brewer-Dobson circulation (Brewer, 1949; Dobson, 1956; Holton et al., 1995). The seasonal variations in the mixing ratio of long-lived gases are conserved during their slow upward transport in the stratosphere as first observed in water vapor by Mote et al. (1995), who termed this phenomenon an atmospheric tape recorder. The signature in water vapor is primarily determined by its seasonally varying entry values at the tropopause (the tape head) which are controlled by temperature. Tape recorders have been found in other trace gases with lifetimes longer than months, such as CO_2 (Andrews et al., 1999), driven by seasonal changes in photosynthesis, and HCN (Pumphrey et al., 2008; Li et al., 2009; Pommrich et al., 2010), driven by the seasonal changes in biomass burning. Schoeberl et al. (2006) identified a tape recorder in CO using satellite measurements from the Aura Microwave Limb Sounder (MLS). In this study, we use a global model to interpret the processes resulting in the observed spatial-temporal variability of the CO tape recorder in the upper troposphere and lower stratosphere (UTLS), taking advantage of the multi-year record now available. This analysis allows us to evaluate vertical transport in the UTLS in the GEOS-4 and GEOS-5 assimilated meteorological fields.

Schoeberl et al. (2006) showed that the structure of the CO tape recorder is closely linked to its seasonal variations in the UT, using MLS data from August 2004 to December 2005. They attributed the peaks in February–April and September–October to biomass burning. Duncan et al. (2007a) examined how the spatial and temporal variations in CO sources as well as troposphere-to-stratosphere transport (TST) impact the composition of the UTLS in a model study. Their chemical transport model (CTM) was driven by meteorological fields from the GEOS-4 general circulation model (GCM) and used a climatological inventory for biomass burning emissions appropriate for the 1980s (Lobert et al., 1999; Duncan et al., 2003). They demonstrated that the seasonal oscillations in UTLS CO result from the combined influence of a semiannual cycle in

ACPD
12, 17397–17442, 2012

CO from biomass burning and an annual cycle in vertical transport, with their conclusions deduced primarily from model simulations. Liu et al. (2007) compared satellite datasets for thin clouds, water vapor and CO near the tropical tropopause and concluded that the spatial and temporal patterns of CO were determined by the influence of seasonal variations of biomass burning and deep convection. Randel et al. (2007) noted a large annual cycle in CO above the tropical tropopause and attributed it to the strong annual cycle in upwelling.

Our study complements and extends previous studies of the CO tape recorder using the multi-year MLS record (Livesey et al., 2011) and simulations with the GEOS-Chem CTM. Our analysis uses both GEOS-4 and GEOS-5 assimilated meteorological fields in the model, and it builds on our earlier study of transport of tropical CO from the lower to the upper troposphere using Aura satellite data (Liu et al., 2010). Our work provides a detailed understanding of the mechanisms responsible for the spatial and temporal patterns of CO in the UTLS and allows us to evaluate vertical transport in the GEOS-4 and GEOS-5 fields in this region. Section 2 of this paper introduces the data and models used in this study. Section 3 evaluates the spatial and vertical distribution of CO in the models using MLS data, presents our analysis of the CO tape recorder, and evaluates vertical transport in UTLS. Our results are discussed in Sect. 4.

2 Data and models

2.1 Satellite data

The MLS instrument is a small radio telescope installed on the front of the Aura satellite, which was launched on 15 July 2004, in a near polar, sun-synchronous orbit with an equator crossing at 01:45 a.m. and 01:45 p.m. local solar time and a 16-day repeat cycle. It continuously measures thermal emission from broad spectral bands (118–2250 GHz) with 7 microwave receivers using a limb viewing geometry (Waters et al., 2006). It performs one scan every 1.5° along the Aura orbit. We use the recently

ACPD
12, 17397–17442, 2012

released Version 3.3 data ranging from August 2004 to February 2012, and apply the screening procedures recommended in the Users' Guide (Livesey et al., 2011). These include the use of a cloud ice-water content (IWC) filter to avoid cloud-contaminated profiles. The data are provided on a fixed pressure grid with 6 levels per decade, with valid CO data at 215, 147, and 100 hPa in the UT. The vertical resolution of the CO product is ~4 km. Comparisons with aircraft CO observations indicated that the earlier version of MLS CO (v2.2) was biased high by a factor of ~2 at 215 hPa (Livesey et al., 2008). This bias has been largely eliminated in v3.3 CO data (Livesey et al., 2012).

2.2 Model description

We use the GEOS-Chem global 3-D model (version 8-02-04, http://www.geos-chem.org/) driven by the GEOS assimilated meteorological observations, GEOS-4 (Bloom et al., 2005) and GEOS-5 (Rienecker et al., 2007). The native resolution of the GEOS-4 fields is $1^\circ \times 1.25^\circ$ with 55 vertical levels, and that of the GEOS-5 fields is $0.5^\circ \times 0.667^\circ$ with 72 vertical levels; we regrid to $2^\circ \times 2.5^\circ$ for input to GEOS-Chem. The vertical resolution of both GEOS-4 and GEOS-5 fields is ~1 km in the UTLS. A major difference between these two meteorological fields is their convective parameterization schemes as discussed by Liu et al. (2010).

In this study, we conducted tagged CO simulations (Duncan et al., 2007b) for January 2004 to December 2010 driven by GEOS-5. For GEOS-4, the simulation spans three years and ends in December 2006, limited by the availability of the meteorological fields in the GEOS-Chem model. The GEOS-4 and GEOS-5 simulations (for 2004–2008) use the same emissions as described in Liu et al. (2010), including the GFED2 emissions for biomass burning (van der Werf et al., 2006). The GFED2 emissions have been used in many recent studies with GEOS-Chem, including those focusing on the tropics (e.g. Sauvage et al., 2007; Nassar et al., 2009; Liu et al., 2010). We also conducted a simulation with the tagged model driven by GEOS-5 using the latest version of the inventory, GFED3 (van der Werf et al., 2010), and this extended the model results to December 2010. The GFED2 and GFED3 emissions for CO are similar, in terms of

ACPD
12, 17397–17442, 2012

the seasonal and interannual variation from 2004 to 2008 over the tropics. The only major difference is over Northern Africa, in which the peak emissions are about 40 % smaller in 2007 in the GFED3 inventory. GFED3 also has slightly lower peak emissions in N. Africa during the other years and in Indonesia in boreal spring 2005. The GFED3 emissions are slightly higher over Southern Africa during its burning season from 2004 to 2008, and are ∼20 % higher over South America in 2005.

Unlike many GEOS-Chem tropospheric studies that use reduced vertical resolution in the stratosphere, the simulations in this study use the model levels at their native vertical resolution. All model simulations have horizontal resolution of $2^{\circ} \times 2.5^{\circ}$ and used monthly mean fields of OH archived from the respective O_3-NO_x-hydrocarbon chemistry simulations, preceded by a three-year spin-up (Liu et al., 2010). The primary chemical loss of CO is through reactions with OH radicals. As a result, the average lifetime for CO in the UT is about 85–120 days in GEOS-4 and 70–85 days in GEOS-5. The chemical production and loss rates of CO in the stratosphere were archived from simulations of the Global Modeling Initiative (GMI) Combo model, which includes a complete treatment of stratospheric photochemistry (e.g. Allen et al., 2010). The CO lifetime in the stratosphere increases slowly with height and reaches a maximum of about 120 days in GEOS-4 and 130 days in GEOS-5 at 60 hPa.

To compare model output with the MLS retrieved profiles, we sampled the model profiles along the MLS orbit track at the observation time, and smoothed the model profiles using the MLS averaging kernel (AK) to interpolate them to the MLS's 37 pressure levels, using the updated AKs for V3.3 (Livesey et al., 2011).

3 Results

3.1 CO morphology in the UTLS

Figure 1 compares the temporal variation of tropical zonal mean CO observed by MLS and simulated by the model driven by GEOS-4 (blue line) and GEOS-5 (red dashed

ACPD
12, 17397–17442, 2012

line) using GFED2 emissions, as well as the run using GFED3 emissions (red solid line). Results are shown for 10° N to 10° S from 215 hPa to 68 hPa. Although the model results are systemically low for most of the six years at 215 hPa, they match the observed CO seasonality in phase and amplitude, with a semi-annual cycle. The amplitude of the models' seasonal variations becomes progressively smaller from 215 hPa to 68 hPa, in contrast to the observed pattern. The phase of the seasonal variation resembles that in the observations at 100 hPa, but by 68 hPa the models peak 2–3 months later in 2005 and fail to simulate the observed peak in January/February. There is an annual cycle in both the observations and the models at 68 hPa. The model results show broader CO peaks and troughs than observed as well as much smaller amplitudes in their seasonal variation. Both models underestimate the observed CO at 100 hPa, especially during boreal winter-spring. Clearly much less CO has been lofted to 68 hPa in GEOS-5 than in GEOS-4, implying insufficient vertical transport in GEOS-5. We return to this issue in more detail in Sect. 3.2. The GEOS-5 simulation with GFED3 emissions shows a small reduction in CO from January to May compared to the simulation with GFED2 emissions, and little difference the rest of the year. This results mainly from the smaller emissions from Northern Africa in GFED3.

Figure 2 shows the spatial distribution of CO from MLS and from the model simulations with GFED2 in February 2005, during the northern biomass burning season; the model results with GFED3 are similar. Both models show CO maxima at 215 hPa over South America, Northern Africa and Indonesia as observed in the MLS data. However, the data show that the primary CO maximum is from Africa, while in the GEOS-4 model it is from Indonesia, and in the GEOS-5 model the maxima from Indonesia and Africa are roughly equivalent. The weak maximum over South America is caused mainly by the accumulated emissions from isoprene with a smaller contribution from biomass burning in the northern part of South America (Liu et al., 2010, Fig. 8). The maximum over Africa is caused by lofting of emissions from fires in Northern Africa in the intertropical convergence zone (ITCZ), as discussed in detail in Liu et al. (2010), while the maximum over Indonesia is caused by lofting of biomass burning emissions from that

ACPD
12, 17397–17442, 2012

region. These CO maxima are collocated with intense convection south of the Equator, which is characterized by high IWC in the MLS data (top panel of Fig. 3). The IWC data are an indicator of convective strength, as stronger convection produces more condensates and larger cloud particles (Jiang et al., 2009). From 146 hPa to 100 hPa, the modeled CO maxima, especially in GEOS-5, show a much larger decrease than those in the MLS CO. However, from 100 hPa to 68 hPa, MLS CO decreases more than does the model CO in both simulations. Carbon monoxide is relatively well mixed in the tropics at 68 hPa.

Figure 4 (top) shows the pressure-latitude cross-section of zonal mean CO in February 2005, highlighting the vertical gradient in tropical CO in the MLS data and model simulations. In the MLS data, CO shows an apparent pipe-like maximum in the tropics from 200 hPa to 100 hPa, with a stronger vertical gradient above 100 hPa than below. In the models, the horizontal gradients are more diffuse in the UT and the vertical gradient of CO is stronger below 100 hPa and weaker above 100 hPa than that in MLS CO as was evident in the maps (Fig. 2).

Figure 5 shows the spatial distribution of CO in July 2005, during the Asian monsoon season. At 215 hPa, the MLS data show that the dominant maximum is over Asia. It is associated with the monsoon circulation and is collocated with intense convection as shown in Fig. 3 (middle panel). Previous studies suggested that the Asian monsoon circulation provides an effective pathway for surface emissions from Asia to enter the global stratosphere, and the MLS data show extremely high CO up to 100 hPa (e.g. Park et al., 2009; Randel et al., 2010). However, both models show a large underestimate throughout the UT over Southeast Asia and Northern Africa. GEOS-4 fails to simulate a CO maximum at 100 hPa.

Although the model CO is too low throughout the UT over Southern and Eastern Asia, this is not caused by the deficiency in model emissions, as the underestimate relative to satellite observations is much less in the lower troposphere in this region as found in our earlier work (Liu et al., 2010). The MLS data shows that there is strong uplift of CO in July between 10° N and 30° N which is lacking in GEOS-4 and

ACPD
12, 17397–17442, 2012

underestimated in GEOS-5 (Fig. 4, center panel). The MOZART model, driven by NCEP meteorology, is more successful at matching this aspect of transport to the UTLS (Park et al., 2009).

The MLS data shows a smaller maximum over Northern Africa at 215 hPa in July. Previous studies suggest that this maximum at ~200 hPa around 10° N is driven by deep convective uplift of CO from biomass burning in Southern Africa (Barret et al., 2008; Liu et al., 2010). There is a large underestimate in both models, caused by an underestimate of emissions of CO from Southern Africa, as well as by deficiencies in vertical transport (Liu et al., 2010). The CO from the southern fires is transported across the Atlantic in the equatorial easterlies, as shown in MLS data. Above ~150 hPa, CO over Northern Africa is influenced by westward transport of pollution from Southeast Asia and India lofted by the Asian summer monsoon (Lelieveld et al., 2002; Liu et al., 2010). The tagged CO results show that outflow from the Asian monsoon anticyclone extends southwestward across the Indian Ocean and merges with the SH subtropical westerlies around the anticyclone located northwest of Australia in the Southern Indian Ocean. This inter-hemispheric transport pathway was discussed in detail in the context of stratospheric ozone by Hitchman and Rogal (2010). The MLS data show CO transport in the westerlies over the Indian Ocean at 15°–20° S, a feature largely lacking in the models' westerly flow. These transport pathways give rise to a C-shaped CO maximum at 100 hPa. However, because of the much weaker uplift of CO over the Asian anticyclone, as well as the underestimate of emissions from Africa, both models show large underestimates over the tropics and also fail to simulate the C-shaped CO maximum. The CO minimum over the equatorial Indian Ocean is caused by lofting of clean boundary layer air by convection.

Results for October 2005, during the southern biomass burning season, are shown in Fig. 6. Clearly, both models underestimate the two major CO maxima over South America and Southern Africa and the smaller peak over the Eastern Indian Ocean that are evident in the MLS data. The pressure-latitude cross-sections show that October is the first month with more CO from the Southern Hemisphere (SH) than from the

ACPD
12, 17397–17442, 2012

Northern Hemisphere (NH) evident in MLS CO (Fig. 4, lower panels). Insufficient CO is transported into the UTLS, and our earlier work showed that this is a combination of an underestimate of biomass burning emissions and of deficiencies in vertical transport (Liu et al., 2010). We evaluated the models with data from the Tropospheric Emission Spectrometer (TES) in the lower troposphere as well as with MLS data in the UT and found that the models were biased low in the lower troposphere and around 215 hPa over both South America and Southern Africa. The run with GFED3 emission shows little difference in tropical zonal mean CO mixing ratios over this season. As in February, MLS CO shows a smaller decrease from 215 hPa to 100 hPa and a greater decrease from 100 hPa to 68 hPa than do the model simulations.

In general, the GEOS-Chem simulations capture the main features of the CO morphology in the UTLS during different seasons (albeit with biases), and these are closely related to the seasonal variation of the biomass burning emissions and to seasonal north-south shifts of regions with strong vertical transport.

3.2 CO tape recorder

Figure 7 shows the tape recorder in CO (as a zonal mean for 10° S to 10° N.). A 4-yr mean (2005–2008) was subtracted from the time series at each level for MLS data and the two GEOS-5 model simulations. For GEOS-4, we removed a reconstructed 4-yr mean calculated by multiplying its 2-yr mean by the ratio of the 4 and 2-yr means in GEOS-5 using GFED2 emissions.

Generally, the models capture the main features shown in the MLS data, although there are differences in detail. The observations and simulations have a semiannual cycle around 200 hPa and a strong annual cycle above 80 hPa. Both MLS observations and model simulations show strong inter-annual variation during the Northern and Southern Hemisphere fire seasons, as also shown in Fig. 1. The strongest CO peak occurs in the boreal autumn of 2006, caused largely by emissions from intense fires in Indonesia (Fig. 8b). In late 2004 and 2010, the MLS data show two other large peaks with nearly the same magnitude as that in late 2006, particularly at 147 hPa and

ACPD
12, 17397–17442, 2012

100 hPa. Maps of CO show that the peak in late 2004 was mainly caused by emissions from fires in both Indonesia and South America, while the peak in late 2010 arose mainly from fires in South America (Fig. 8a and 8d). Several recent studies discussed the severe drought in 2010 in South America (and associated intense fire activity) and attributed it to the combined influence of a strong El Nino in 2009 and early 2010 and an extremely warm tropical North Atlantic in 2010 (Chen et al., 2011; Fernandes et al., 2011; Lewis et al., 2011). The model simulations capture the observed CO maximum in late 2006 and are slightly too low for the 2004 maximum, but the results using GFED3 emissions are significantly too low for late 2010. We showed in Liu et al. (2010) that there is insufficient upward transport over South America in GEOS-5 at the start of the wet season, and this, combined with too low emissions, probably explains the discrepancy.

During the northern burning season, the largest CO positive anomaly occurs in 2005, a result of emissions from fires in Northern Africa and Indonesia as shown in Fig. 2. Use of the GFED3 emissions leads to a small reduction in the overestimate of the peaks in early 2005 (by ~2 ppb over Northern Africa and ~4–5 ppb over Indonesia) compared to the results with GFED2 emissions.

To understand the causes of the observed spatial-temporal pattern in CO, we first examine the CO sources and vertical transport around 215 hPa. This is about the level with maximum outflow from convection (e.g. Fueglistaler et al., 2009). The CO signals near 200 hPa provide the boundary condition (or the tape head) for CO entering the UTLS. Figure 9 shows time series of tagged CO tracers for a model level at 226 hPa over the tropics from individual sources, including biomass burning sources from the various continents, the biogenic source from isoprene, and the sources from fossil fuel combustion, for GEOS-4 (black lines), GEOS-5 using GFED2 emissions (red dashed lines), and GEOS5 using GFED3 emissions (red solid lines). The source of CO from isoprene oxidation persists throughout the year and has little seasonal or interannual variation. Isoprene emissions are larger in GEOS-5 than in GEOS-4 (not shown), and the associated CO in GEOS-4 exceeds that in GEOS-5 by about 20 %

ACPD
12, 17397–17442, 2012

as a consequence. The source of CO from oxidation of CH_4 is about 30 ppb in both GEOS-4 and GEOS-5, and seasonally and interannually invariant (not shown). The CO from fossil fuel use persists all year, varying seasonally and reaching a maximum (~17 ppb) in boreal winter and a minimum (~10 ppb) in boreal autumn. Duncan et al. (2007a) found a similar seasonality for this source in their GCM study. The fossil fuel CO from Asia is the largest major contribution to this seasonal variation in the models (not shown). The tropical CO minimum from fossil fuel occurs during the Asian monsoon season, when pollutants are trapped north of 10° N in the lower layer and vertically transported to higher levels above the tropopause (Fig. 5, e.g. Park et al., 2009). Figure 9 shows that fossil fuel emissions provides the dominant contribution to CO to the inner tropics in northern summer, and the underestimate in this season evident in Fig. 1 is clearly related to the models' transport problems over Asia discussed above. The maximum in the fossil fuel source occurs in boreal winter, when deep convection moves southward to the tropics and transports more CO emissions from Southeastern Asia to the tropics below the tropopause.

Emissions from biomass burning on the different continents display characteristic seasonal cycles in the UT, with a maximum in late boreal winter resulting from fires in Northern Africa and in boreal summer-autumn from fires in Southern Africa and South America. Thus the temporal overlap from these continents generates much of the semi-annual cycle in CO at 200 hPa in Fig. 7. The contributions from fires in Southeast Asia are not shown in Fig. 9, as they are always less than 3 ppb.

The strong inter-annual variation of tropical mean CO during the southern biomass burning season is controlled primarily by the interannual variation of fires in Indonesia and South America, which are both strongly influenced by climate related dynamic variability. Previous studies showed that fires are most severe in Indonesia during drought conditions (e.g. Van Nieuwstadt and Sheil, 2005), which are generally associated with El Niño events (e.g. Ropelewski and Halpert, 1987; Curtis et al., 2001). Several recent studies suggest that droughts in Indonesia are also affected by the phase of the Indian Ocean Dipole (IOD). For example, the huge fires in Indonesia in late 2006 were

ACPD
12, 17397–17442, 2012

attributed to the combined strength of El Niño and a strongly positive phase of the IOD (e.g. Field and Shen, 2008; van der Werf et al., 2008; Field et al., 2009; Nassar et al., 2009). In both late 2004 and 2009, two other El Niño periods, the IOD was in a neutral phase as inferred from the Dipole Mode Index (DMI) (Figure S1). Thus, CO emissions from Indonesian fires in these two years were much smaller than in 2006, even though the 2009 El Nino was slightly stronger than that in 2006. As a result, there are much smaller peaks at 215 hPa in 2004 and 2009 than in 2006 (Figs. 8 and 9). The CO emissions from South American fires were at a minimum in late 2009, and thus the tropical mean CO is much smaller in late 2009 than that in late 2004 (Fig. 7). As discussed above, the late 2010 peak is mainly caused by CO from fires in South America. Adoption of the GFED3 emissions improved the underestimate of the CO maximum in late 2006 with GFED2 emissions by ∼5 ppb, but led to little difference compared to results with GFED2 emissions during the southern biomass burning season in other years.

The interannual variation of tropical zonal mean CO during the northern biomass burning season is affected mainly by fires in Northern Africa and Indonesia. We note that the simulations with GFED2 exaggerate the contribution of the Indonesian fires in early 2005, as shown in Fig. 2, probably a result of too high emissions. The run with GFED3 shows a reduction of ∼4–5 ppb in zonal mean CO from Indonesia for this period. The simulations with GFED3 emissions show a ∼2–5 ppb decrease in zonal mean CO originating from Northern Africa fires during January and February between 2005 and 2008 compared to those with GFED2 emissions. In 2005, the smaller GFED3 emissions from Northern Africa fires reduce the model overestimate with GFED2 emissions, but in other years they exacerbate the model underestimates.

Propagation of the tape recorder signal depends on vertical transport in the models. Figure 10a shows the monthly variation of the tropical zonal mean vertical velocity at 226 hPa. This is calculated from the upward air mass flux associated with convection and with vertical advection (the pressure tendency) in the CTM. We compute vertical velocities from the air mass flux. The CTM is driven by 6-h-time-averaged horizontal winds from the GEOS data assimilation system (Pawson et al., 2007) and advection is

ACPD
12, 17397–17442, 2012

calculated in the CTM by a conservative flux-form upstream-based transport scheme (Lin and Rood, 1996). Both GEOS-4 and GEOS-5 have a strong seasonal cycle with the maximum upward mass flux in April and May, a relatively weak secondary peak in November and December, and a minimum in July to September. The vertical velocities in the CTM driven by GEOS-4 are approximately twice those using GEOS-5 at 226 hPa.

Figure 11 shows the CO tape recorder for the MLS retrieval levels to facilitate detailed evaluation of the models. The model simulations and observations agree reasonably well at 215 and 147 hPa, with clear semi-annual cycles. At 100 hPa, a semi-annual cycle exists in the data, but in the simulations the peak late in the year is very weak or missing. At 68 hPa a pronounced annual cycle is present in the data with a maximum in January/February, extending into May in 2005, while the simulations display much smaller amplitude, and the peak is about 3 months late. Clearly the seasonal variation starts changing to an annual cycle at too low an altitude in the models. Between 68 hPa and 46 hPa, the annual cycle in MLS CO changes phase from a minimum in August to November to a maximum in these months at 46 hPa. Such a change is absent in the phase of the model simulations, with a relatively weak annual cycle and a CO maximum in March to June at both levels. The CO data from the infrared Atmospheric Chemistry Experiment-Fourier Transform Spectrometer (ACE-FTS) (Boone et al., 2005) have a high signal-to-noise ratio at 46 hPa, allowing independent evaluation of MLS CO at this level. Similar to the model simulations, the ACE-FTS data for CO have the same phase at 46 hPa as at 68 hPa, and have a much smaller amplitude than the MLS data at 46 hPa (K. Walker and H. Pumphrey, personal communication, 2011). Given these differences at 46 hPa, we do not use the MLS data for higher altitudes. We note that the ACE-FTS data are less useful for analysis of the CO tape recorder because they have sparse temporal sampling in the tropics and fail to capture the semi-annual cycle at 215 hPa.

Figure 11 also highlights the different propagation rates of the CO signal from fires in the NH and SH evident in the MLS data. From 147 hPa to 68 hPa, the CO peak from NH fires shows a lag of 0–2 months, while that from the SH fires shows a lag of

ACPD
12, 17397–17442, 2012

3–4 months. Both peaks show a slower propagation from 100 hPa to 68 hPa than from 147 hPa than 100 hPa. The difference in the phase lags for CO peaks that originate in late winter and in early autumn increases with height, and around 68 hPa, the two peaks coalesce and the semi-annual cycle shifts to an annual cycle. Thus, the single peak in the MLS data in January–May at 68 hPa is caused by the superposition of the CO maxima from fires in the NH and SH due to the different propagation rates, with a faster ascent rate in boreal winter.

Figure 10b and 10c show the monthly variation of the vertical velocities in the CTM at 100 hPa and 67 hPa. Both models show a similar seasonal cycle with annual and semi-annual harmonics as shown at 226 hPa, with a maximum in March to May and minimum in July to August. The vertical velocities calculated from the air mass divergence scheme in the CTM are larger in December to May, consistent with the extra-tropical wave-driven pump theory (Holton et al., 1995) and also consistent with seasonal variation of vertical velocities deduced from radiative heating rates calculated from observed water vapor and ozone using a radiative transfer model (Yang et al., 2008). The vertical velocities in GEOS-5 are much smaller than those in GEOS-4 in all seasons from 226 hPa to 67 hPa. Thus much less CO is lofted to 68 hPa in GEOS-5 than in GEOS-4, even though the two models have similar CO at 215 hPa (Fig. 1). However, the CO tape recorder, which is normalized by the mean value, shows similar results for the two models, implying that the models' tape recorder pattern above ~150 hPa depends more on the phase than on the magnitude of the vertical transport.

The lower panels of Fig. 10 show that the vertical profile of the seasonal mean vertical velocity has a minimum around 70–80 hPa, causing the maximum lag of the models' CO peak to occur from 100 hPa to 68 hPa. The transport minimum occurs at a lower altitude in June to November, with mean velocities close to zero in GEOS-5, and this, coupled with the seasonality in the vertical velocity in the UTLS (top panels), causes the much slower and less effective propagation of the October maximum from SH fires (e.g. in 2006) than the peaks in February/March (e.g. in 2005 and 2007).

ACPD
12, 17397–17442, 2012

The transport time from 215 hPa to 100 hPa is about 20–50 days in the GEOS-4 model and 48–80 days in the GEOS-5 model, shorter than the CO chemical lifetimes of about 100 days and 80 days, respectively. The transport time from 100 hPa to 68 hPa is about 58 days in GEOS-4 and 94 days in GEOS-5 in December–May, becoming comparable to the seasonal mean chemical lifetime of 93 days and 88 days, respectively at least for GEOS-5. The transport time in June–November is about 166 days and 228 days in GEOS-4 and GEOS-5, longer than its chemical lifetime. Thus the CO mixing ratios in both models are influenced by both photochemical and transport processes by around 68 hPa, especially in boreal summer, and the tape recorder is no longer dominated by transport processes alone.

3.3 Vertical velocity derived from daily MLS CO fields

Schoeberl et al. (2008) used 15 yr of satellite measurements of tropical H_2O to estimate the vertical velocities in the UTLS by correlating the H_2O phase lag between two adjacent levels. Their empirically deduced vertical transport rates represent the net effects of the vertical and horizontal eddy transport as well as the mean large-scale vertical transport. We adopted their method and deduced the vertical ascent rate of the CO extrema in Fig. 11 using the MLS observations. Figure 12a shows the daily tropical zonal mean MLS CO deviations from 215 hPa to 21 hPa. The general patterns of rising CO maxima and minima are obvious. To extract vertical velocities from the CO extrema, we first isolate the pattern of rising CO deviations from other patterns including the measurement noise. We performed an extended empirical orthogonal function (EOF) analysis on the daily time-height series in Fig. 12a to extract the vertical propagation of CO peaks driven by the seasonal cycle of upwelling. Unlike the standard EOF analysis, the extended EOF technique extracts the temporal evolution of the spatial pattern. Further details about this method can be found in analyses of stratospheric winds (Fraedrich et al., 1993; Mote et al., 1995; Wang et al., 1995).

In our study, we first apply a 6-month running window to the time-height matrix and generate an extended matrix with a maximum lag of 10 months; we then apply

ACPD
12, 17397–17442, 2012

a standard EOF analysis to the extended matrix to obtain the time development of the vertical structure. The first two EOFs show a seasonal cycle containing the annual and semi-annual harmonics simulating the propagation of CO maxima in spring and autumn. Together they account for 45 % of the total variance. The third and fourth EOFs show the temporal evolution of spatial patterns for a semi-annual and bi-annual cycle and account for 15 % and 12 % of the total variance, respectively. We calculate a normalized convolution of the first three EOFs with their respective temporal coefficients to reconstruct an altitude-temporal pattern of MLS CO (Fig. 12b). In the resulting plot, the ascending minima and maxima of CO retain their identity from ~200 hPa to 30 hPa.

We deduce the vertical velocity directly by calculating the phase-lagged correlation coefficients between two adjacent levels following the method used in Schoeberl et al. (2008). The calculation uses the reconstructed daily MLS data shown in Fig. 12b. The temporal lagged correlation is calculated for a window of 3 months for pressures greater than 68 hPa and 6 months for pressures at and less than 68 hPa; these windows correspond to about a half of the wavelength of the tape recorder signal below and above 68 hPa, respectively. For each temporal window we calculate the correlation coefficients between the data at the lower level and the phase-shifted data at the upper level with one day increments up to 10 months, and identify the lag time with the highest correlation. The vertical velocity is then calculated by dividing the distance between two levels by the lag-time with the highest correlation; it is assigned to the mid-point of two levels. We follow the filtering criteria used by Schoeberl et al. (2008) and we remove occurrences of maximum correlation between two levels above 100 hPa of less than 10 days. We show the profile of vertical velocities deduced from MLS CO from 2005 to 2006 with those archived in GEOS-4 and GEOS-5 at pressures greater than 68 hPa (Fig. 13), because of lack of confidence in the seasonal cycle at 46 hPa in the MLS data, and because of potential effects of photochemical loss of CO. The vertical velocities inferred from MLS CO show a reasonable seasonality with a faster ascent rate in the winter-spring season at pressures greater than 90 hPa. The MLS vertical velocity in June-November exceeds that in boreal winter at around 90 hPa and above,

ACPD
12, 17397–17442, 2012

which is in conflict with results from previous studies (e.g. Mote et al., 1995; Rosenlof, 1995; Schoeberl et al., 2008; Yang et al., 2008). This is probably caused by the influence of chemical loss of CO at 68 hPa in boreal summer and fall as discussed above. Thus, we argue that this method is most useful for deriving vertical velocities in the UT, which is a key advantage of using CO as a tracer of transport. It extends our quantification of vertical transport to the lower part of the TTL. Previous studies based on H_2O focus on levels above 100 hPa because that is where the tape head is set by the tropopause temperature (Mote et al., 1995, 1998). The GMI CTM does not transport H_2O above the tropopause. The ascent rates calculated from CO are $\sim$1.0 mm s^{-1} in DJF and $\sim$0.54 mm s^{-1} in SON at $\sim$125 hPa, which are in reasonable agreement with those deduced from other long lived tracers around 100 hPa using CO_2 (Park et al., 2010) and H_2O (Mote et al., 1998), as well as those deduced from radiative heating rates (Yang et al., 2008) (Fig. 13).

The vertical velocities derived from MLS CO in the UT are larger than those derived from the archived GEOS-5 fields in all seasons. They agree well with those from archived GEOS-4 fields between 215 hPa and 125 hPa except in boreal spring, when the vertical velocity derived from MLS CO is much larger than that calculated from the GEOS-4 fields. The ascent rates from MLS CO decrease more slowly with height and exceed those from the GEOS-4 fields at $\sim$125 hPa. Thus as shown in Fig. 1, transport of CO from 215 hPa to 147 hPa is similar to that of MLS CO, but not enough CO is transported up to 100 hPa because the vertical velocities in both models are too low at this level.

Both models underestimate MLS CO at 100 hPa throughout 2004 to 2008, but this is not the case at 68 hPa, especially in the GEOS-4 model from April to November (Fig. 1). This seems to present a conundrum, since we argue above that the models' vertical transport is too slow at these levels. Examining the contributions from the tagged sources at 68 hPa (Fig. 14), we found that sources from biomass burning and isoprene oxidation are at their minimum from May to September and increase to their seasonal maximum in December to April. Methane oxidation is the largest source of

ACPD
12, 17397–17442, 2012

CO at 68 hPa and accounts for more than 50 % of the total CO throughout the year. It has a relatively strong seasonal cycle with a maximum in March to May and a minimum in August to October, which follows the annual cycle of upwelling (Fig. 10). Fossil fuel combustion, originating mainly from NH mid-latitudes, is the second largest source of CO at 68 hPa year round. The contribution of CO from methane oxidation and fossil fuel increases from ~45 % at 226 hPa to ~70 % at 68 hPa from May to November. The model matches the MLS data at 68 hPa when CO from these two sources contribute the most to total CO, and underestimates CO during December to March when insufficient CO from tropical biomass burning and isoprene oxidation has been lofted upwards. At 100 hPa, where the models are too low year-round, CO from biomass burning and isoprene constitute a larger fraction of total CO. The vertical velocities deduced from MLS H_2O by Schoeberl et al. (2008) imply that the minimum in vertical transport is at 20–22 km, or 40–50 hPa. However in both GEOS fields, the minimum occurs at ~100 hPa to 80 hPa in June–November and ~68 hPa in December–May as shown above (Fig. 10d, e), and hence there is inadequate upward transport of the CO sources that originate in the tropical troposphere, as discussed above.

The mean vertical velocities from both models for 10° N–10° S are extremely low above 100 hPa in June–November. This is particularly evident in GEOS-5, with mean downward, rather than upward motion in boreal summer. As shown in Fig. 1, the CO maximum from fires in the SH is much less than that in MLS CO above 147 hPa in both model simulations. This maximum almost disappears by 100 hPa due to the extremely low ascent rate in the models. Both models show a broader but weaker CO maximum from January to May.

4 Discussion and conclusions

We used the GEOS-Chem model to investigate the impacts of surface emissions and dynamical processes on the spatial and temporal patterns of CO in the tropical UTLS observed from MLS. During the northern biomass burning season, the CO maxima in

ACPD
12, 17397–17442, 2012

February and March arise from biomass burning emissions from the north of South America, Northern Africa, and Indonesia, lofted by intense convection which takes place primarily to the south of the Equator. Maps of MLS CO, as well as the tagged CO simulations, show that emissions from Southeast Asia contribute little to the CO maximum during this period. This conclusion is in contrast to the model results of Duncan et al. (2007a), who attributed the CO maximum in March to emissions from fires in Southeast Asia, a conclusion resulting from the underlying inventory (Lobert et al., 1999), which greatly overestimated biomass burning in that region (Heald et al., 2004).

During the Asian monsoon season both GEOS-4 and GEOS-5 underestimate the observed CO maximum at 100 hPa that extends from the Middle East to the Tibetan Plateau, where the CO is trapped in the anti-cyclonic circulation (e.g. Li et al., 2005; Park et al., 2007). This appears to be related to insufficient lofting of Asian CO emissions by convection and associated uplift to ~200 hPa over the Indian Ocean, and the problem is worse in GEOS-4. Another consequence of the insufficient lofting is that very little CO from Asia is transported to the southwest, across the Indian Ocean, and around the anticyclone in the Southern Indian Ocean into the westerlies, so that the models fail to simulate the CO maximum observed in MLS data at 15°–20° S. A third consequence is that insufficient CO is transported around the Asian anticyclone towards North Africa, and this, combined with an underestimate of emissions of CO from Southern Africa and insufficient vertical transport in the ITCZ (Liu et al., 2010) gives rise to an underestimate of CO over Central and Northern Africa and the Atlantic Ocean during the Asian monsoon season.

During the southern biomass burning season, the CO maxima in September to November result from biomass burning emissions from South America and Southern Africa. The model simulations of the CO maxima above these regions are generally low in the UTLS due to combined influence of insufficient surface emissions and vertical transport in the model.

The MLS observation shows a pipe-like CO maximum in the tropics between 200 and 100 hPa, isolated to a narrow latitude band from January to April (Fig. 4a shows the

ACPD
12, 17397–17442, 2012

situation in February), when tropical upward motion reaches its seasonal maximum. However, the CO distribution is broader and less isolated in the tropics in both models, which may be caused by too slow ascent and stronger in-mixing from higher latitudes. The CO maxima in the models decrease faster below 100 hPa (~16 km) and slower above compared to the MLS observations, implying that the vertical transport in the model decays at a lower altitude than in the atmosphere, or that the horizontal mixing is too strong above 100 hPa, or a combination of both. This hypothesis was further verified by comparing the vertical velocities deduced from MLS CO to those derived from the archived GEOS-4 and GEOS-5 meteorological fields by mass continuity. The vertical velocities derived by tracking the propagation of MLS CO extrema agree well with those for the GEOS-4 fields between 215 hPa and 125 hPa in boreal summer, autumn and winter, and exceed those in GEOS-4 fields at pressures less than 125 hPa, resulting in limited CO transport up to 100 hPa in the models. Schoeberl et al. (2008) also suggested that the vertical velocities both in models driven by GEOS-4 GCM and derived from the meteorological fields in the data assimilation system (DAS) have a transport minimum at a lower altitude compared to the vertical velocities deduced from MLS H_2O. However, the vertical velocities shown for the GEOS-4 DAS in Schoeberl et al. (2008) were calculated from averaged net heating rates (M. Schoeberl, personal communication, 2010). These are not used to transport tracers in the off-line CTM where the vertical transport is calculated from the archived horizontal winds by mass continuity and from the convective mass fluxes in the troposphere.

For GEOS-5, the transport is slower than that deduced from MLS CO in all seasons and is downwards above 100 hPa in tropics in boreal summer, which appears to conflict with the well-known tropical upward transport (Holton et al., 1995). A recent back trajectory analysis (Ploeger et al., 2010), conducted to test the impact of the various vertical velocity scenarios on transport in the UTLS, showed that almost no subsidence occurred in the UTLS in a diabatic scenario with the cross-isentropic velocities deduced from different diabatic heating rates; however subsidence frequently appeared in a kinematic scenario, commonly used in off-line CTM models, with the

ACPD
12, 17397–17442, 2012

pressure tendency used for the vertical transport. It is not clear whether this subsidence in the tropics is real or an artifact of the kinematic scenario. Spatial maps of the tropical vertical velocity fields in GEOS-4 and GEOS-5 are very similar to those in the ERA-Interim kinematic vertical wind fields depicted in Ploeger et al. (2010), their Fig. 6, showing similar spatial patterns of downward and upward transport. Park et al. (2007) also show regions of downward and upward transport at 100 hPa in the tropics in the ERA40 reanalysis in July/August (their Fig. 12). Evidently the GEOS assimilated fields are not unique in having these vertical transport patterns in the tropics.

One of interpretations for the steeper CO gradient with slower vertical transport below 100 hPa may be the inherent characteristics of the transport scheme used in CTMs. Waugh et al. (1997) compared the simulations of various long-lived gases between an on-line transport model, which calculates the wind fields as well as the tracer fields, and an off-line transport model, which reads in the assimilated meteorological fields and derives the vertical velocity by mass continuity. They identified a difference in simulated vertical gradients of long-lived tracers in the stratosphere between off-line and on-line models. The weaker CO gradient above 100 hPa in both models used here may also indicate excessive mixing from the extra-tropics into the lower stratosphere, considering that there is insufficient vertical transport at these levels when using GEOS assimilated meteorological fields in the off-line CTM.

Both simulations and observations of the tropical zonal mean CO deviation have a semi-annual cycle around 200 hPa and a strong annual cycle above 80 hPa. Liu et al. (2007) argued that the semiannual cycle in CO results from the overlap of seasonal variations in deep convective transport and biomass burning emissions, based on the comparison of satellite observations for thin clouds, water vapor and CO near tropical tropopause. Our tagged CO simulations show that the semi-annual cycles of CO below 80 hPa in the TTL are determined by the temporal overlapping of surface biomass burning emissions from different continents as well as the north-south shifts of deep convection regions. Both GEOS-4 and GEOS-5 have a strong seasonal cycle with the maximum upward transport in April and May and a minimum in July to

ACPD
12, 17397–17442, 2012

September. The CO peaks from NH fires propagate faster to the LS than do those from SH fires. Thus the transition from a semi-annual to an annual cycle around 80 hPa is induced by a combination of the CO signal at the tropopause and the annual cycle of the Brewer-Dobson circulation in the lower stratosphere. In GEOS-5, the shift to an annual cycle occurs at an altitude lower than that in MLS CO, a result of inadequate upward transport in the UT. As shown above, the mean vertical velocities from both models for 10° N–10° S are lower than those inferred from MLS CO above 100 hPa in June–November. This is particularly evident in GEOS-5, with mean downward, rather than upward, motion in boreal summer. Thus the CO maxima from SH burning in both model simulations are transported less effectively than those in MLS CO above 147 hPa and almost disappear by 100 hPa. At 68 hPa, the CO from SH burning is too low to coalesce with the peak from the NH fires, and the model lacks strong maxima in January/February seen in the data, producing a broader but weaker CO maximum from January to May in both models. By 68 hPa, due to the decreased ascent rate, the transport time becomes comparable to the CO photochemical lifetime, especially in boreal summer-fall, and the spatial and temporal structures of CO are affected by both processes.

Both model simulations and MLS observations have a strong inter-annual variation with a CO maximum in boreal fall 2006, caused mainly by fires in the Indonesian region, as well as a peak in boreal spring 2005, contributed by fires in Indonesia and Northern Africa. The maximum in late 2004 was caused mainly by emissions from fires in Indonesia and South America, while that in late 2010 arose mainly from fires in South America induced by a severe climatic-driven drought in 2010. As a result of the insufficient vertical transport over South America in GEOS-5 as well as an underestimate of emissions from that continent, the model underestimates both the maximum in 2004 and particularly that in 2010.

Although the large-scale vertical transport in GEOS-5 is insufficient and much weaker than that in GEOS-4, the CO tape recorder patterns show a matched phase of upward propagation between GEOS-4 and GEOS-5. We argue that this is possibly

ACPD
12, 17397–17442, 2012

caused by the compensating contributions from the tropical recirculation in GEOS-5. Strahan et al. (2009) examined the transport characteristics of tropical recirculation using the age spectra. They suggested that the difference between the mean age and modal age of tropical air indicates the strength of recirculation into the tropics. A stronger recirculation leads to a wider mode width and an older mean age. Simulations with both GEOS-5 and GEOS-4 match the observed seasonality of the CO tape recorder in phase from 215 to 100 hPa, which indicates that they have similar transit times of CO extremes and furthermore similar derived vertical velocities to those deduced from MLS observations. Previous studies suggest that the derived ascent rate from the upward propagation rate of long-lived gases deviations is directly related to the modal age in a low vertical transport environment (Hall and Waugh, 1997; Waugh and Hall, 2002). As a result, both GEOS-4 and GEOS-5 have a similar modal age, which is also shown in their age spectra (S. Strahan, personal communication, 2011). The age spectrum experiment also suggests that the mean age of air in GEOS-5 is older than that in GEOS-4. Thus GEOS-5 has a larger difference between its mean and modal age, indicating greater recirculation into the tropical pipe in the LS, which diminishes the CO maximum in GEOS-5. Consequently, the simulations with GEOS-5 show a matched phase of upward propagation, but much less CO is lofted to 68 hPa compared to those in GEOS-4.

Clearly the CO tape recorder provides valuable tests of vertical transport in 3-D models, particularly in the UT, below the altitudes where the H_2O tape recorder tests transport, and below where age of air is most useful as a transport diagnostic. We recommend that the CO tape recorder is implemented as a transport test in models driven by both assimilated fields, nudged GCM fields, and GCM fields. Such a test could use the GFED3 emissions and prescribed OH fields, if they are not available in the models.

ACPD
12, 17397–17442, 2012

Supplementary material related to this article is available online at: http://www.atmos-chem-phys-discuss.net/12/17397/2012/acpd-12-17397-2012-supplement.pdf.

Acknowledgements. This work was funded by NASA grant NNX10AG59G to Harvard University. Work at the Jet Propulsion Laboratory, California Institute of Technology, was performed under contract with NASA. We acknowledge helpful discussions with S. Strahan on age spectra analysis of GEOS-4 and GEOS-5, and we thank D. B. A. Jones for enlightening us about interhemispheric transport across the Indian Ocean in boreal summer. We also thank M. Niwano, M. Schoeberl, and K. Walker for helpful discussions.

References

Allen, D., Pickering, K., Duncan, B., and Damon, M.: Impact of lightning NO emissions on North American photochemistry as determined using the Global Modeling Initiative (GMI) model, J. Geophys. Res.-Atmos., 115, D22301, doi:10.1029/2010jd014062, 2010.

Andrews, A. E., Boering, K. A., Daube, B. C., Wofsy, S. C., Hintsa, E. J., Weinstock, E. M., and Bui, T. P.: Empirical age spectra for the lower tropical stratosphere from in situ observations of CO_2: implications for stratospheric transport, J. Geophys. Res.-Atmos., 104, 26581–26595, 1999.

Barret, B., Ricaud, P., Mari, C., Attié, J.-L., Bousserez, N., Josse, B., Le Flochmoën, E., Livesey, N. J., Massart, S., Peuch, V.-H., Piacentini, A., Sauvage, B., Thouret, V., and Cammas, J.-P.: Transport pathways of CO in the African upper troposphere during the monsoon season: a study based upon the assimilation of spaceborne observations, Atmos. Chem. Phys., 8, 3231–3246, doi:10.5194/acp-8-3231-2008, 2008.

Bloom, S., da Silva, A., Dee, D., Bosilovich, M., Chern, J.-D., Pawson, S., Schubert, S., Sienkiewicz, M., Stajner, I., Tan, W.-W., and Wu, M.-L.: Documentation and Validation of the Goddard Earth Observing System (GEOS) Data Assimilation System - Version 4, Technical Report Series on Global Modeling and Data Assimilation Rep., NASA Goddard Space Flight Center, Md, 2005.

ACPD

12, 17397–17442, 2012

Boone, C. D., Nassar, R., Walker, K. A., Rochon, Y., McLeod, S. D., Rinsland, C. P., and Bernath, P. F.: Retrievals for the atmospheric chemistry experiment Fourier-transform spectrometer, Appl. Optics., 44, 7218–7231, 2005.

Brewer, A. W.: Evidence for a world circulation provided by the measurements of helium and water vapour distribution in the stratosphere, Q. J. Roy. Meteorol. Soc., 75, 351–363, 1949.

Chen, Y., Randerson, J. T., Morton, D. C., DeFries, R. S., Collatz, G. J., Kasibhatla, P. S., Giglio, L., Jin, Y. F., and Marlier, M. E.: Forecasting fire season severity in South America using sea surface temperature anomalies, Science, 334, 787–791, doi:10.1126/science.1209472, 2011.

Curtis, S., Adler, R., Huffman, G., Nelkin, E., and Bolvin, D.: Evolution of tropical and extratropical precipitation anomalies during the 1997–1999 ENSO cycle, Int. J. Climatol., 21, 961–971, 2001.

Dobson, G. M. B.: Origin and distribution of the polyatomic molecules in the atmosphere, Proc. Roy. Soc. A, 236, 187–193, 1956.

Duncan, B. N., Martin, R. V., Staudt, A. C., Yevich, R., and Logan, J. A.: Interannual and seasonal variability of biomass burning emissions constrained by satellite observations, J. Geophys. Res.-Atmos., 108, D24100, doi:10.1029/2002jd002378, 2003.

Duncan, B. N., Strahan, S. E., Yoshida, Y., Steenrod, S. D., and Livesey, N.: Model study of the cross-tropopause transport of biomass burning pollution, Atmos. Chem. Phys., 7, 3713–3736, doi:10.5194/acp-7-3713-2007, 2007a.

Duncan, B. N., Logan, J. A., Bey, I., Megretskaia, I. A., Yantosca, R. M., Novelli, P. C., Jones, N. B., and Rinsland, C. P.: Global budget of CO, 1988–1997: source estimates and validation with a global model, J. Geophys. Res.-Atmos., 112, D22301, doi:10.1029/2007jd008459, 2007b.

Fernandes, K., Baethgen, W., Bernardes, S., DeFries, R., DeWitt, D. G., Goddard, L., Lavado, W., Lee, D. E., Padoch, C., Pinedo-Vasquez, M., and Uriarte, M.: North Tropical Atlantic influence on Western Amazon fire season variability, Geophys. Res. Lett., 38, L12701, doi:10.1029/2011gl047392, 2011.

Field, R. D. and Shen, S. S. P.: Predictability of carbon emissions from biomass burning in Indonesia from 1997 to 2006, J. Geophys. Res.-Biogeo., 113, G04024, doi:10.1029/2008jg000694, 2008.

ACPD
12, 17397–17442, 2012

Field, R. D., van der Werf, G. R., and Shen, S. S. P.: Human amplification of drought-induced biomass burning in Indonesia since 1960, Nat. Geosci., 2, 185–188, doi:10.1038/NGEO443, 2009.

Fraedrich, K., Pawson, S., and Wang, R. S.: An eof analysis of the vertical time-delay structure of the quasi-biennial oscillation, J. Atmos. Sci., 50, 3357–3365, 1993.

Fueglistaler, S., Dessler, A. E., Dunkerton, T. J., Folkins, I., Fu, Q., and Mote, P. W.: Tropical tropopause layer, Rev. Geophys., 47, RG1004, doi:10.1029/2008rg000267, 2009.

Hall, T. M. and Waugh, D. W.: Timescales for the stratospheric circulation derived from tracers, J. Geophys. Res.-Atmos., 102, 8991–9001, 1997.

Heald, C. L., Jacob, D. J., Jones, D. B. A., Palmer, P. I., Logan, J. A., Streets, D. G., Sachse, G. W., Gille, J. C., Hoffman, R. N., and Nehrkorn, T.: Comparative inverse analysis of satellite (MOPITT) and aircraft (TRACE-P) observations to estimate Asian sources of carbon monoxide, J. Geophys. Res.-Atmos., 109, D23306, doi:10.1029/2004jd005185, 2004.

Hitchman, M. H. and Rogal, M. J.: ENSO influences on Southern Hemisphere column ozone during the winter to spring transition, J. Geophys. Res.-Atmos., 115, D20104, doi:10.1029/2009jd012844, 2010.

Holton, J. R., Haynes, P. H., Mcintyre, M. E., Douglass, A. R., Rood, R. B., and Pfister, L.: Stratosphere–troposphere exchange, Rev. Geophys., 33, 403–439, 1995.

Jiang, J. H., Su, H., Massie, S. T., Colarco, P. R., Schoeberl, M. R., and Platnick, S.: Aerosol–CO relationship and aerosol effect on ice cloud particle size: analyses from Aura Microwave Limb Sounder and Aqua Moderate Resolution Imaging Spectroradiometer observations, J. Geophys. Res.-Atmos., 114, D20207, doi:10.1029/2009jd012421, 2009.

Lelieveld, J., Berresheim, H., Borrmann, S., Crutzen, P. J., Dentener, F. J., Fischer, H., Feichter, J., Flatau, P. J., Heland, J., Holzinger, R., Korrmann, R., Lawrence, M. G., Levin, Z., Markowicz, K. M., Mihalopoulos, N., Minikin, A., Ramanathan, V., de Reus, M., Roelofs, G. J., Scheeren, H. A., Sciare, J., Schlager, H., Schultz, M., Siegmund, P., Steil, B., Stephanou, E. G., Stier, P., Traub, M., Warneke, C., Williams, J., and Ziereis, H.: Global air pollution crossroads over the Mediterranean, Science, 298, 794–799, 2002.

Lewis, S. L., Brando, P. M., Phillips, O. L., van der Heijden, G. M. F., and Nepstad, D.: The 2010 Amazon drought, Science, 331, 554–554, doi:10.1126/science.1200807, 2011.

ACPD

12, 17397–17442, 2012

Li, Q., Palmer, P. I., Pumphrey, H. C., Bernath, P., and Mahieu, E.: What drives the observed variability of HCN in the troposphere and lower stratosphere?, Atmos. Chem. Phys., 9, 8531–8543, doi:10.5194/acp-9-8531-2009, 2009.

Li, Q. B., Jiang, J. H., Wu, D. L., Read, W. G., Livesey, N. J., Waters, J. W., Zhang, Y. S., Wang, B., Filipiak, M. J., Davis, C. P., Turquety, S., Wu, S. L., Park, R. J., Yantosca, R. M., and Jacob, D. J.: Convective outflow of South Asian pollution: a global CTM simulation compared with EOS MLS observations, Geophys. Res. Lett., 32, L14826, doi:10.1029/2005gl022762, 2005.

Lin, S. J. and Rood, R. B.: Multidimensional flux-form semi-Lagrangian transport schemes, Mon. Weather Rev., 124, 2046–2070, 1996.

Liu, C. T., Zipser, E., Garrett, T., Jiang, J. H., and Su, H.: How do the water vapor and carbon monoxide "tape recorders" start near the tropical tropopause?, Geophys. Res. Lett., 34, L09804, doi:10.1029/2006gl029234, 2007.

Liu, J., Logan, J. A., Jones, D. B. A., Livesey, N. J., Megretskaia, I., Carouge, C., and Nedelec, P.: Analysis of CO in the tropical troposphere using Aura satellite data and the GEOS-Chem model: insights into transport characteristics of the GEOS meteorological products, Atmos. Chem. Phys., 10, 12207–12232, doi:10.5194/acp-10-12207-2010, 2010.

Livesey, N. J., Filipiak, M. J., Froidevaux, L., Read, W. G., Lambert, A., Santee, M. L., Jiang, J. H., Pumphrey, H. C., Waters, J. W., Cofield, R. E., Cuddy, D. T., Daffer, W. H., Drouin, B. J., Fuller, R. A., Jarnot, R. F., Jiang, Y. B., Knosp, B. W., Li, Q. B., Perun, V. S., Schwartz, M. J., Snyder, W. V., Stek, P. C., Thurstans, R. P., Wagner, P. A., Avery, M., Browell, E. V., Cammas, J. P., Christensen, L. E., Diskin, G. S., Gao, R. S., Jost, H. J., Loewenstein, M., Lopez, J. D., Nedelec, P., Osterman, G. B., Sachse, G. W., and Webster, C. R.: Validation of Aura Microwave Limb Sounder O_3 and CO observations in the upper troposphere and lower stratosphere, J. Geophys. Res.-Atmos., 113, D15S02, doi:10.1029/2007jd008805, 2008.

Livesey, N. J., Read, W. G., Froidevaux, L., Lambert, A., Manney, G. L., Pumphrey, H. C., Santee, M. L., Schwartz, M. J., Wang, S., Cofield, R. E., Cuddy, D. T., Fuller, R. A., Jarnot, R. F., Jiang, J. H., Knosp, B. W., Stek, P. C., Wagner, P. A., and Wu, D. L.: EOS MLS Version 3.3 Level 2 data quality and description document, Tech. Rep., Jet Propulsion Laboratory, 2011.

Livesey, N. J., Logan, J. A., Santee, M. L., Waters, J. W., Doherty, R. M., Read, W. G., Froidevaux, L., and Jiang, J. H.: Interrelated variations of O_3, CO and deep convection in the

ACPD
12, 17397–17442, 2012

tropical/subtropical upper troposphere observed by the Aura Microwave Limb Sounder (MLS) during 2004–2011, Atmos. Chem. Phys. Discuss., in press, 2012.
Lobert, J. M., Keene, W. C., Logan, J. A., and Yevich, R.: Global chlorine emissions from biomass burning: reactive chlorine emissions inventory, J. Geophys. Res.-Atmos., 104, 8373–8389, 1999.
Mote, P. W., Rosenlof, K. H., Holton, J. R., Harwood, R. S., and Waters, J. W.: Seasonal variations of water-vapor in the tropical lower stratosphere, Geophys. Res. Lett., 22, 1093–1096, 1995.
Mote, P. W., Dunkerton, T. J., McIntyre, M. E., Ray, E. A., Haynes, P. H., and Russell, J. M.: Vertical velocity, vertical diffusion, and dilution by midlatitude air in the tropical lower stratosphere, J. Geophys. Res.-Atmos., 103, 8651–8666, 1998.
Nassar, R., Logan, J. A., Megretskaia, I. A., Murray, L. T., Zhang, L., and Jones, D. B. A.: Analysis of tropical tropospheric ozone, carbon monoxide, and water vapor during the 2006 El Niño using TES observations and the GEOS-Chem model, J. Geophys. Res.-Atmos., 114, D17304, doi:10.1029/2009jd011760, 2009.
Park, M., Randel, W. J., Gettelman, A., Massie, S. T., and Jiang, J. H.: Transport above the Asian summer monsoon anticyclone inferred from Aura Microwave Limb Sounder tracers, J. Geophys. Res.-Atmos., 112, D16309, doi:10.1029/2006jd008294, 2007.
Park, M., Randel, W. J., Emmons, L. K., and Livesey, N. J.: Transport pathways of carbon monoxide in the Asian summer monsoon diagnosed from Model of Ozone and Related Tracers (MOZART), J. Geophys. Res.-Atmos., 114, D08303, doi:10.1029/2008jd010621, 2009.
Park, S., Atlas, E. L., Jiménez, R., Daube, B. C., Gottlieb, E. W., Nan, J., Jones, D. B. A., Pfister, L., Conway, T. J., Bui, T. P., Gao, R.-S., and Wofsy, S. C.: Vertical transport rates and concentrations of OH and Cl radicals in the Tropical Tropopause Layer from observations of CO_2 and halocarbons: implications for distributions of long- and short-lived chemical species, Atmos. Chem. Phys., 10, 6669–6684, doi:10.5194/acp-10-6669-2010, 2010.
Pawson, S., Stajner, I., Kawa, S. R., Hayashi, H., Tan, W. W., Nielsen, J. E., Zhu, Z., Chang, L. P., and Livesey, N. J.: Stratospheric transport using 6-h-averaged winds from a data assimilation system, J. Geophys. Res.-Atmos., 112, D23103, doi:10.1029/2006jd007673, 2007.
Ploeger, F., Konopka, P., Gunther, G., Grooss, J. U., and Muller, R.: Impact of the vertical velocity scheme on modeling transport in the tropical tropopause layer, J. Geophys. Res.-Atmos., 115, D03301, doi:10.1029/2009jd012023, 2010.

ACPD
12, 17397–17442, 2012

Pommrich, R., Muller, R., Grooss, J. U., Gunther, G., Konopka, P., Riese, M., Heil, A., Schultz, M., Pumphrey, H. C., and Walker, K. A.: What causes the irregular cycle of the atmospheric tape recorder signal in HCN?, Geophys. Res. Lett., 37, L16805, doi:10.1029/2010gl044056, 2010.

Pumphrey, H. C., Boone, C., Walker, K. A., Bernath, P., and Livesey, N. J.: Tropical tape recorder observed in HCN, Geophys. Res. Lett., 35, L05801, doi:10.1029/2007gl032137, 2008.

Randel, W. J., Park, M. J., Wu, F., and Livesey, N.: A large annual cycle in ozone above the tropical tropopause linked to the Brewer-Dobson circulation, J. Atmos. Sci., 64, 4479–4488, doi:10.1175/2007jas2409.1, 2007.

Randel, W. J., Park, M., Emmons, L., Kinnison, D., Bernath, P., Walker, K. A., Boone, C., and Pumphrey, H.: Asian monsoon transport of pollution to the stratosphere, Science, 328, 611–613, doi:10.1126/science.1182274, 2010.

Rienecker, M., Suarez, M., Todling, R., Bacmeister, J., Takacs, L., Liu, H., Gu, W., Sienkiewicz, M., Koster, R., Gelaro, R., Stajner, I., and Nielsen, E.: The GEOS-5 Data Assimilation System – Documentation of Versions 5.0.1, 5.1.0, and 5.2.0, Technical Report, Series on Global Modeling and Data Assimilation, NASA/TM-2007-104606, 2007.

Ropelewski, C. F. and Halpert, M. S.: Global and regional scale precipitation patterns associated with the El-Niño southern oscillation, Mon. Weather Rev., 115, 1606–1626, 1987.

Rosenlof, K. H.: Seasonal cycle of the residual mean meridional circulation in the stratosphere, J. Geophys. Res.-Atmos., 100, 5173–5191, 1995.

Sauvage, B., Martin, R. V., van Donkelaar, A., Liu, X., Chance, K., Jaeglé, L., Palmer, P. I., Wu, S., and Fu, T.-M.: Remote sensed and in situ constraints on processes affecting tropical tropospheric ozone, Atmos. Chem. Phys., 7, 815–838, doi:10.5194/acp-7-815-2007, 2007.

Schoeberl, M. R., Duncan, B. N., Douglass, A. R., Waters, J., Livesey, N., Read, W., and Filipiak, M.: The carbon monoxide tape recorder, Geophys. Res. Lett., 33, L12811, doi:10.1029/2006gl026178, 2006.

Schoeberl, M. R., Douglass, A. R., Stolarski, R. S., Pawson, S., Strahan, S. E., and Read, W.: Comparison of lower stratospheric tropical mean vertical velocities, J. Geophys. Res.-Atmos., 113, D24109, doi:10.1029/2008jd010221, 2008.

Strahan, S. E., Schoeberl, M. R., and Steenrod, S. D.: The impact of tropical recirculation on polar composition, Atmos. Chem. Phys., 9, 2471–2480, doi:10.5194/acp-9-2471-2009, 2009.

ACPD
12, 17397–17442, 2012

van der Werf, G. R., Randerson, J. T., Giglio, L., Collatz, G. J., Kasibhatla, P. S., and Arellano Jr., A. F.: Interannual variability in global biomass burning emissions from 1997 to 2004, Atmos. Chem. Phys., 6, 3423–3441, doi:10.5194/acp-6-3423-2006, 2006.

van der Werf, G. R., Dempewolf, J., Trigg, S. N., Randerson, J. T., Kasibhatla, P. S., Gigliof, L., Murdiyarso, D., Peters, W., Morton, D. C., Collatz, G. J., Dolman, A. J., and DeFries, R. S.: Climate regulation of fire emissions and deforestation in equatorial Asia, Proc. Natl. Acad. Sci., 105, 20350–20355, doi:10.1073/pnas.0803375105, 2008.

van der Werf, G. R., Randerson, J. T., Giglio, L., Collatz, G. J., Mu, M., Kasibhatla, P. S., Morton, D. C., DeFries, R. S., Jin, Y., and van Leeuwen, T. T.: Global fire emissions and the contribution of deforestation, savanna, forest, agricultural, and peat fires (1997–2009), Atmos. Chem. Phys., 10, 11707–11735, doi:10.5194/acp-10-11707-2010, 2010.

Van Nieuwstadt, M. G. L. and Sheil, D.: Drought, fire and tree survival in a Borneo rain forest, East Kalimantan, Indonesia, J. Ecol., 93, 191–201, doi:10.1111/j.1365-2745.2004.00954.x, 2005.

Wang, R. S., Fraedrich, K., and Pawson, S.: Phase-space characteristics of the tropical stratospheric quasi-biennial oscillation, J. Atmos. Sci., 52, 4482–4500, 1995.

Waters, J. W., Froidevaux, L., Harwood, R. S., Jarnot, R. F., Pickett, H. M., Read, W. G., Siegel, P. H., Cofield, R. E., Filipiak, M. J., Flower, D. A., Holden, J. R., Lau, G. K. K., Livesey, N. J., Manney, G. L., Pumphrey, H. C., Santee, M. L., Wu, D. L., Cuddy, D. T., Lay, R. R., Loo, M. S., Perun, V. S., Schwartz, M. J., Stek, P. C., Thurstans, R. P., Boyles, M. A., Chandra, K. M., Chavez, M. C., Chen, G. S., Chudasama, B. V., Dodge, R., Fuller, R. A., Girard, M. A., Jiang, J. H., Jiang, Y. B., Knosp, B. W., LaBelle, R. C., Lam, J. C., Lee, K. A., Miller, D., Oswald, J. E., Patel, N. C., Pukala, D. M., Quintero, O., Scaff, D. M., Van Snyder, W., Tope, M. C., Wagner, P. A., and Walch, M. J.: The Earth Observing System Microwave Limb Sounder (EOS MLS) on the Aura satellite, IEEE T. Geosci. Remote., 44, 1075–1092, doi:10.1109/tgrs.2006.873771, 2006.

Waugh, D. W. and Hall, T. M.: Age of stratospheric air: theory, observations, and models, Rev. Geophys., 40, 1010. doi:10.1029/2000rg000101, 2002.

Waugh, D. W., Hall, T. M., Randel, W. J., Rasch, P. J., Boville, B. A., Boering, K. A., Wofsy, S. C., Daube, B. C., Elkins, J. W., Fahey, D. W., Dutton, G. S., Volk, C. M., and Vohralik, P. F.: Three-dimensional simulations of long-lived tracers using winds from MACCM2, J. Geophys. Res.-Atmos., 102, 21493–21513, 1997.

ACPD
12, 17397–17442, 2012

Yang, Q., Fu, Q., Austin, J., Gettelman, A., Li, F., and Vömel, H.: Observationally derived and general circulation model simulated tropical stratospheric upward mass fluxes, J. Geophys. Res., 113, D00B07, doi:10.1029/2008JD009945, 2008.

ACPD
12, 17397–17442, 2012

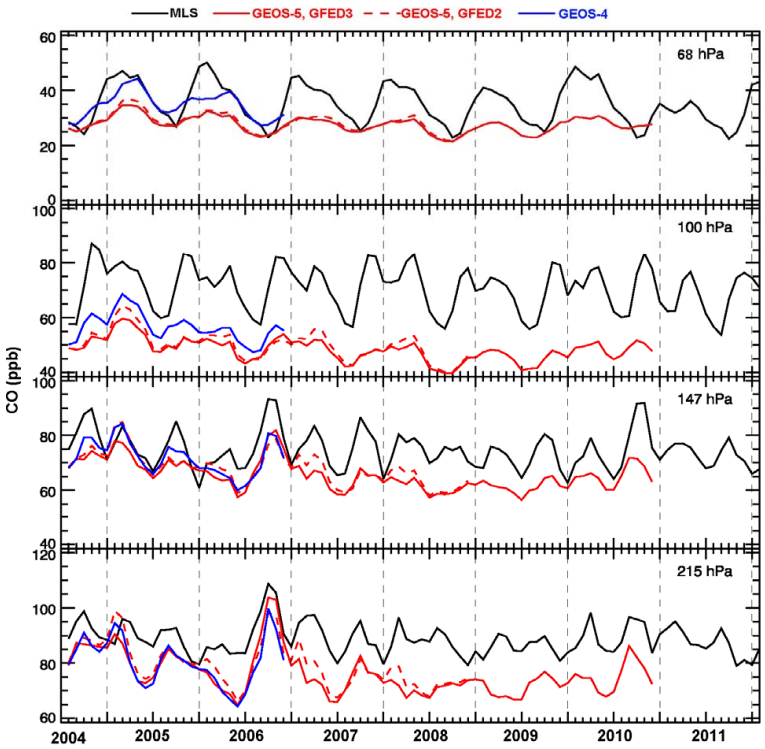

Fig. 1. Temporal variation of tropical zonal mean (10° S to 10° N) MLS CO and model CO mixing ratio at level 215 hPa, 147 hPa, 100 hPa and 68 hPa. Black lines represent MLS observations. Red solid lines represent model results from GEOS-5 using GFED3 emissions. Red dashed lines represent model results from GEOS-5 using GFED2 emissions. Blue lines represent model results from GEOS-4 using GFED2 emissions.

ACPD
12, 17397–17442, 2012

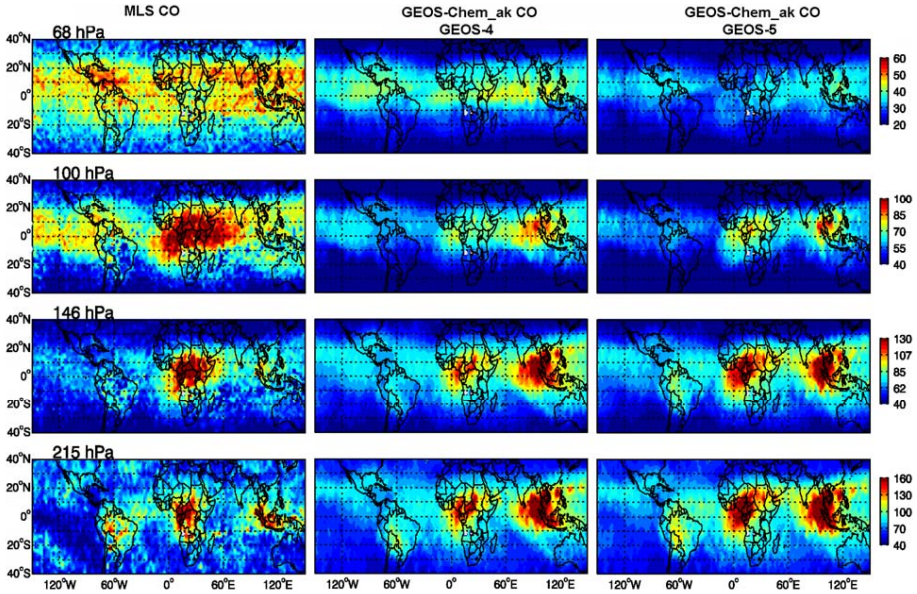

Fig. 2. Spatial patterns of CO mixing ratio at level 215 hPa, 147 hPa, 100 hPa and 68 hPa for February 2005 during the Northern Hemisphere biomass burning season from MLS (left), the GEOS-Chem model simulations driven by GEOS-4 (middle) and GEOS-5 (right) using GFED2 emissions with the MLS AKs applied.

ACPD
12, 17397–17442, 2012

Transport analysis and source attribution of UTLS CO

Junhua Liu et al.

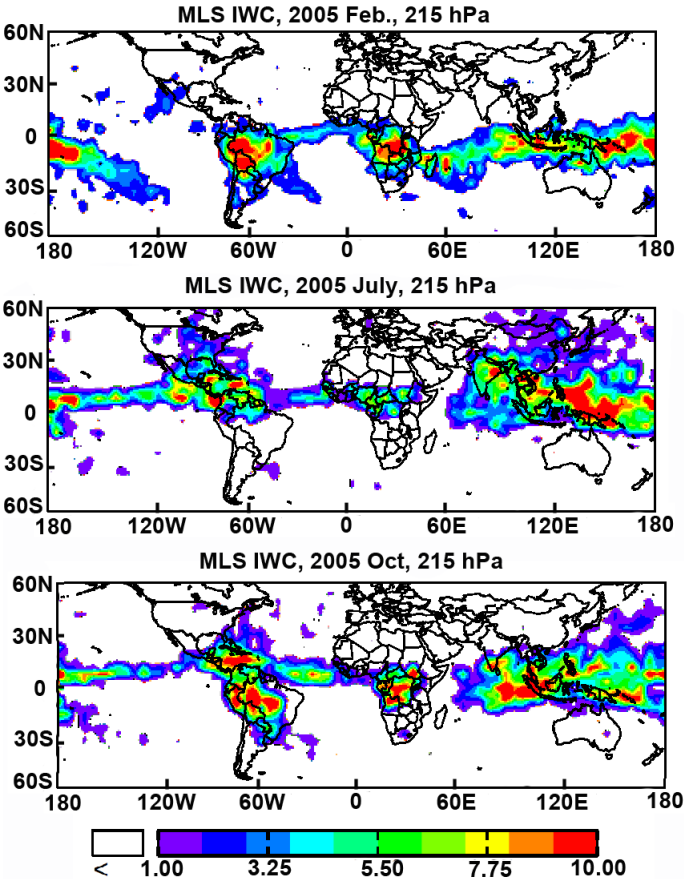

Fig. 3. MLS ice water content (IWC) ($g\,m^{-3}$) at 215 hPa in February (top), July (middle) and October (bottom) 2005.

ACPD
12, 17397–17442, 2012

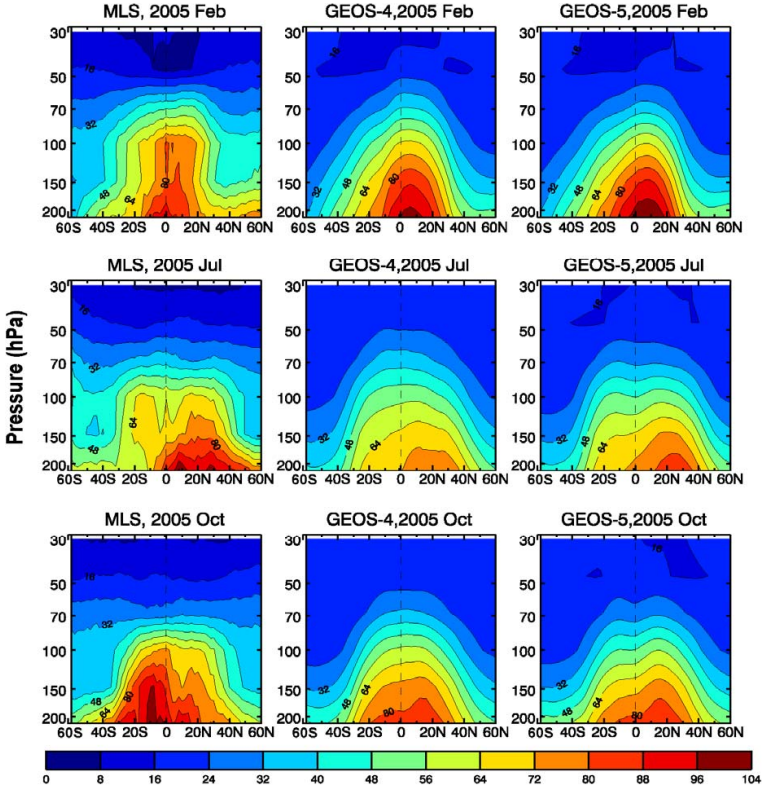

Fig. 4. Pressure-latitude cross-section of zonal mean CO mixing ratio from MLS (left), the GEOS-Chem simulations driven by GEOS-4 (middle) and GEOS-5 (right) using GFED2 emissions with the MLS AKs applied in (top) February, (middle) July and (bottom) October 2005.

ACPD
12, 17397–17442, 2012

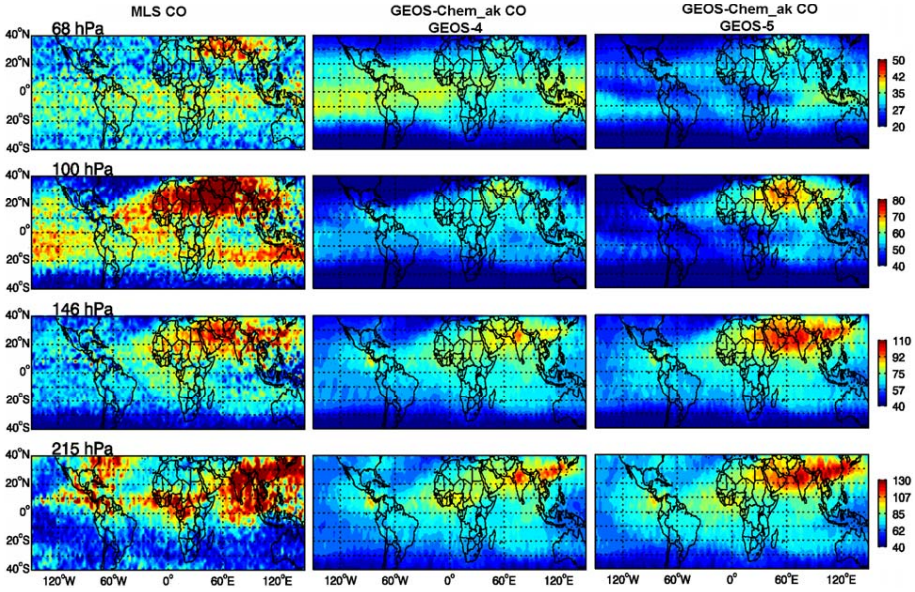

Fig. 5. Spatial patterns of CO mixing ratio at level 215 hPa, 147 hPa, 100 hPa and 68 hPa for July 2005 during the Asian monsoon season from MLS (left), the GEOS-Chem simulations driven by GEOS-4 (middle) and GEOS-5 (right) using GFED2 emissions with the MLS AKs applied.

ACPD
12, 17397–17442, 2012

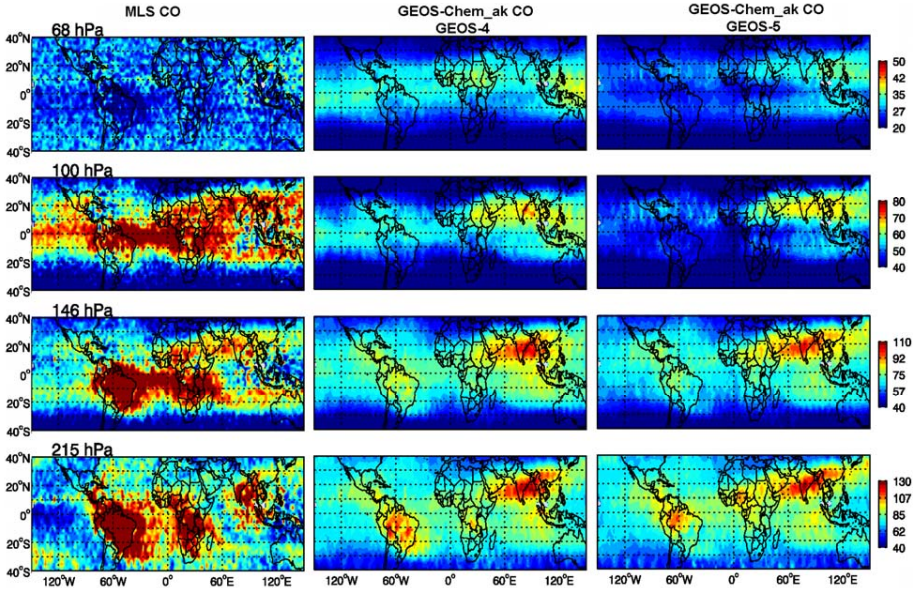

Fig. 6. Spatial patterns of CO mixing ratio at level 215hPa, 147 hPa, 100 hPa and 68 hPa for October 2005 during the Southern Hemisphere biomass burning season from MLS (left), the GEOS-Chem simulations driven by GEOS-4 (middle) and GEOS-5 (right) with the MLS AKs applied.

ACPD
12, 17397–17442, 2012

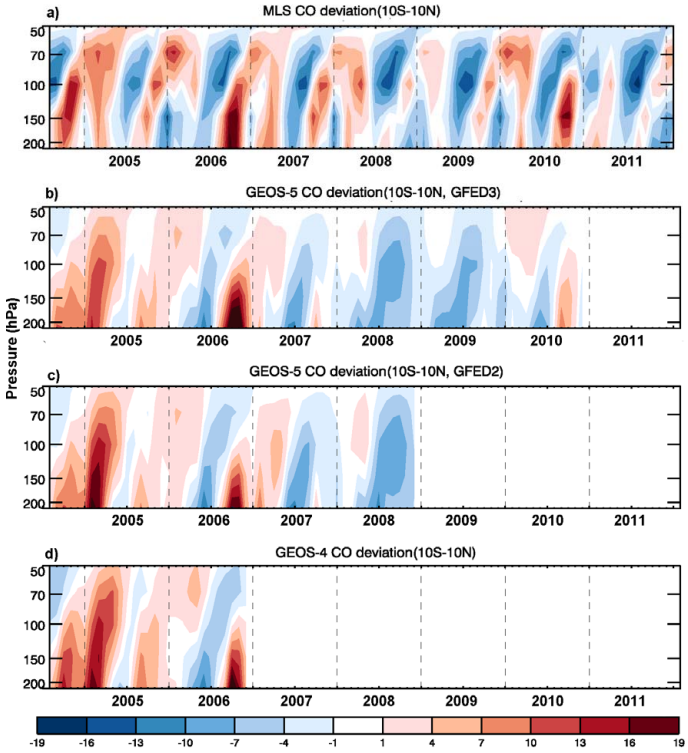

Fig. 7. Temporal variation of tropical zonal mean CO (10° S to 10° N) deviation of **(a)** MLS observations from August 2004 to February 2012 from 200 hPa to 50 hPa, model simulations driven by GEOS-5 with **(b)** GFED3 emission ends in December 2010, **(c)** GFED2 emissions ends in December 2008, and **(d)** GEOS-4 ends in December 2006. The 4-yr mean (2005 to 2008) is subtracted from the time series at each level. The reconstructed 4-yr mean of GEOS-4 is calculated from GEOS-4 2-yr zonal mean multiplying the ratio of GEOS-5 4-yr and 2-yr zonal means.

ACPD
12, 17397–17442, 2012

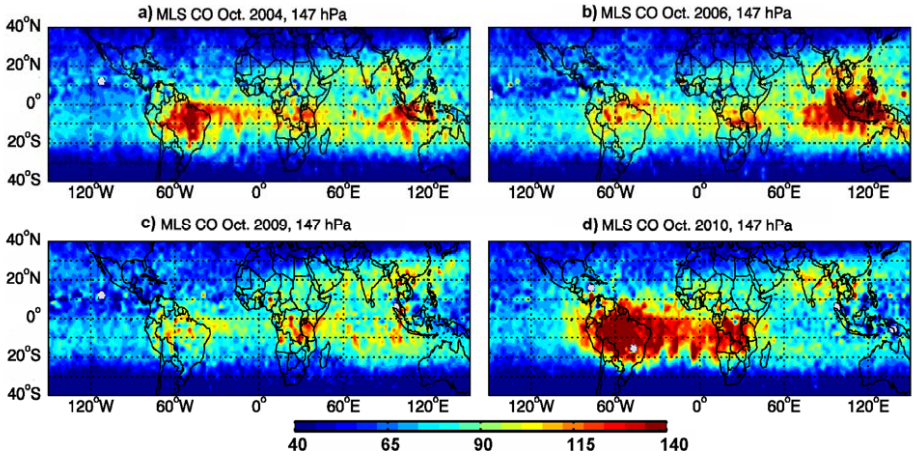

Fig. 8. Spatial patterns of MLS CO mixing ratio at 147 hPa for October 2004, 2006, 2009 and 2010 during the Southern Hemisphere biomass burning season.

ACPD
12, 17397–17442, 2012

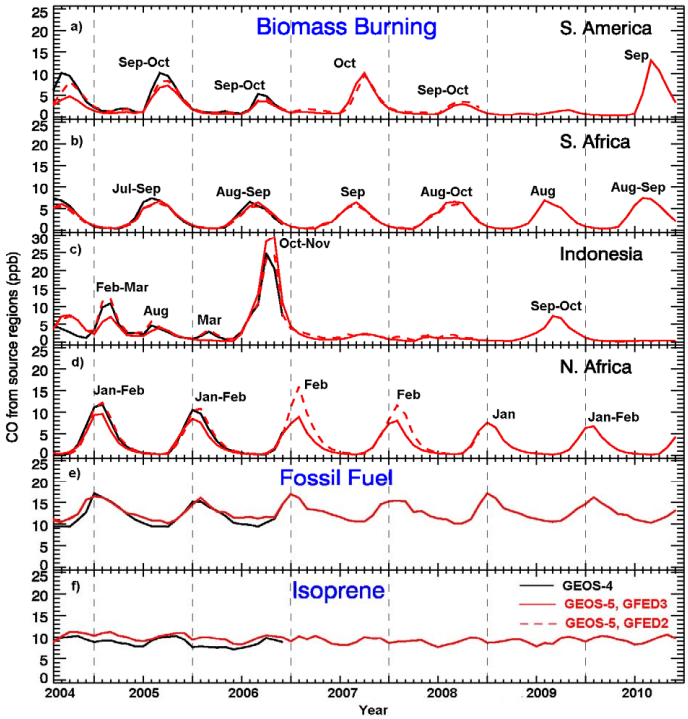

Fig. 9. Temporal variation of modeled tropical zonal mean CO mixing ratio (10° S to 10° N) at 215 hPa from surface biomass burning of **(a)** South America, **(b)** Southern Africa, **(c)** Northern Africa, and **(d)** Indonesia at 215 hPa, showing the boundary condition for CO entering the stratosphere. Panel **(e)** shows the CO variation from Fossil Fuel. **(f)** shows the CO variation from isoprene. Red solid lines represent model results from GEOS-5 with GFED3 emissions. Red dashed lines represent model results from GEOS-5 with GFED2 emissions. Black lines represent model results from GEOS-4.

ACPD
12, 17397–17442, 2012

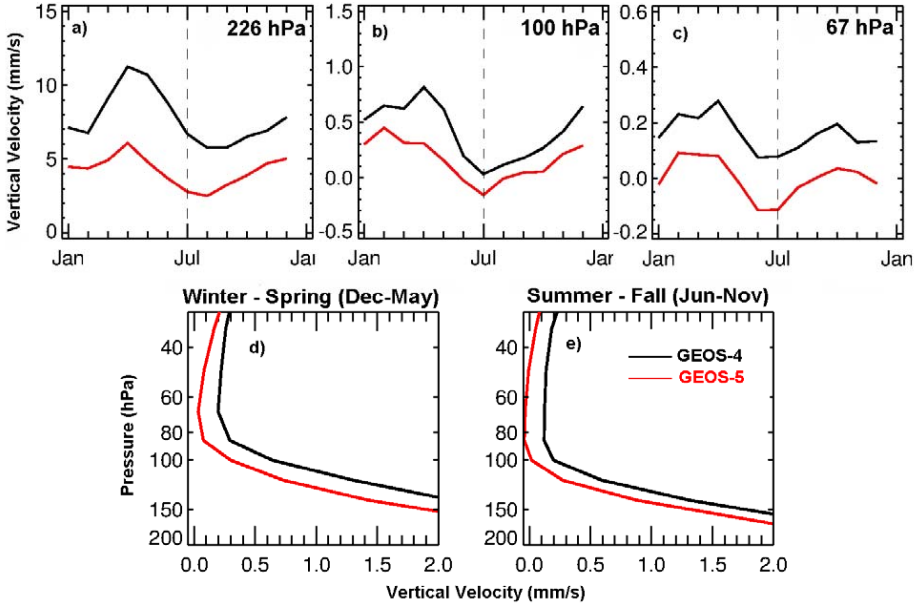

Fig. 10. Monthly variation of the tropical (10° S–10° N) vertical velocity at **(a)** 226 hPa, **(b)** 100 hPa, and **(c)** 67 hPa. Vertical profile of seasonal mean vertical velocity during **(d)** boreal winter-spring (December to May) and **(e)** boreal summer-fall (June to November). Red lines represent model results from GEOS-5. Black lines represent model results from GEOS-4.

ACPD
12, 17397–17442, 2012

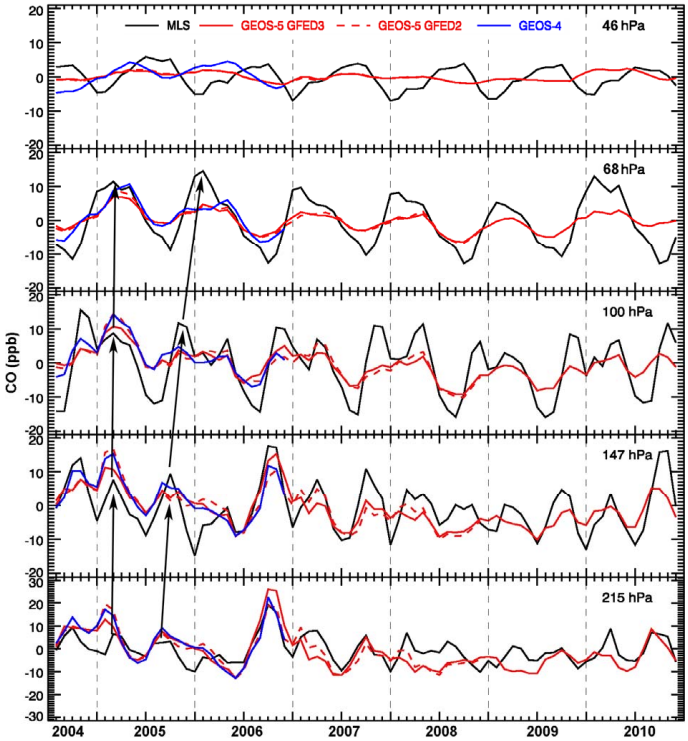

Fig. 11. Temporal variation of tropical (10° S–10° N) MLS CO and model CO anomaly at level 215 hPa, 147 hPa, 100 hPa, 68 hPa and 46 hPa. Black lines represent MLS observations. Red solid lines represent model results from GEOS-5 with GFED3 emissions. Red dashed lines represent model results from GEOS-5 with GFED2 emissions. Blue lines represent model results from GEOS-4. Arrows represent the vertical transport pathways of CO maximum from Southern Hemisphere biomass burning and northern hemisphere biomass burning.

ACPD
12, 17397–17442, 2012

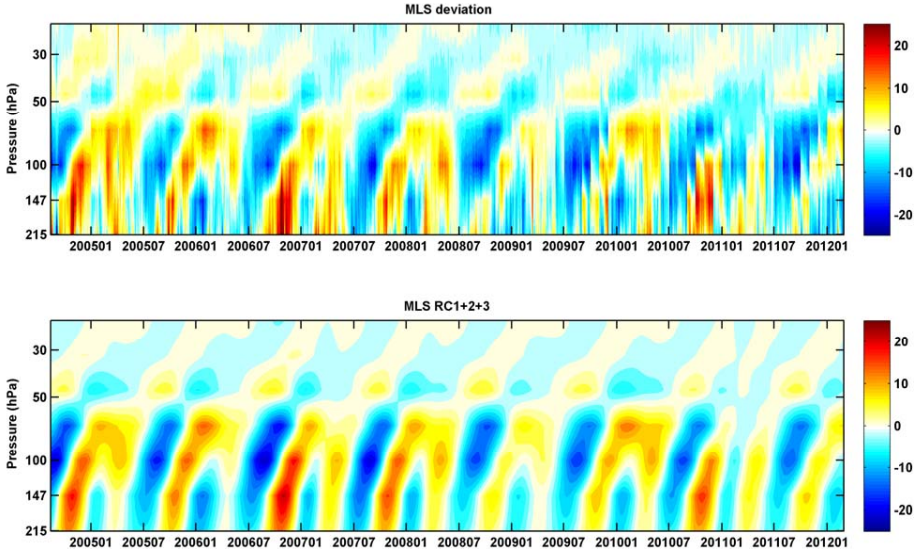

Fig. 12. (top) MLS tropical (10° S–10° N) CO and (bottom) its reconstruction from the first three EEOF from August 2004 to February 2012.

ACPD
12, 17397–17442, 2012

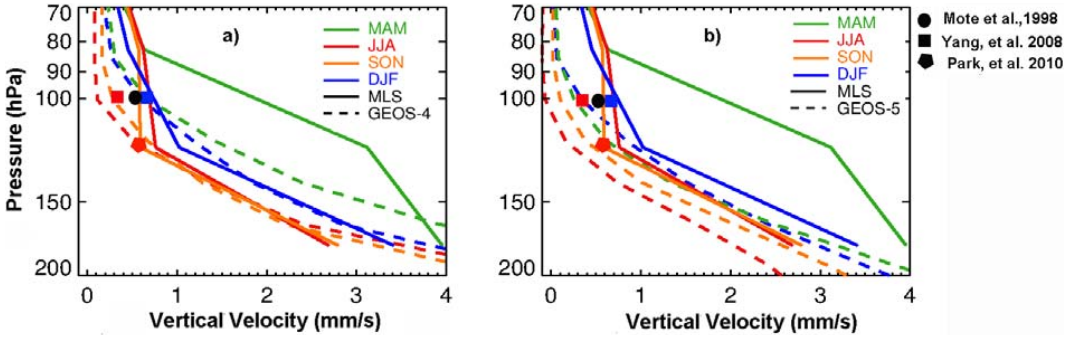

Fig. 13. Comparison of seasonal mean profiles of vertical velocity deduced from reconstructed MLS CO mixing ratio (solid lines) and **(a)** GEOS-4 (dashed lines), **(b)** GEOS-5 (dashed lines) assimilated meteorological fields. Black dot represents the tropical annual mean vertical velocity deduced from MLS H_2O (Mote et al., 1998). Square represents the seasonal mean vertical velocity deduced from radiative heat rate (Yang et al., 2008). Pentagon represents the vertical velocity deduced from CO_2 (Park et al., 2010). Red represents summer season. Blue represents winter season.

ACPD
12, 17397–17442, 2012

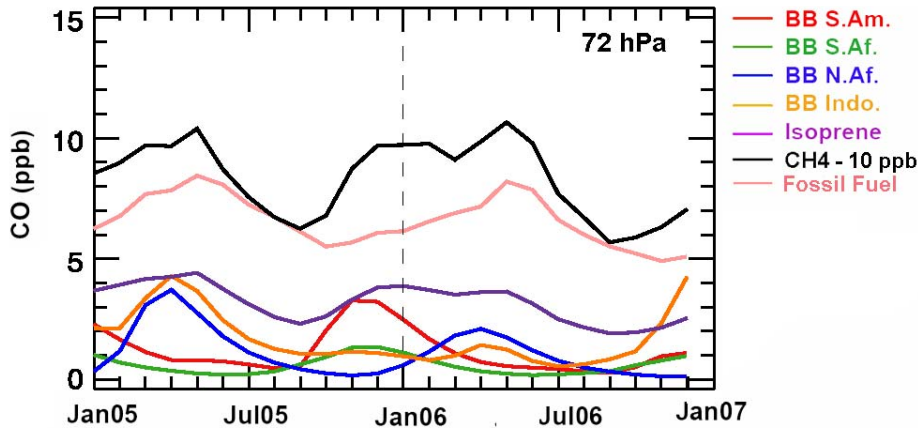

Fig. 14. Time series of tagged CO tracers over tropics (11° S to 11° N) from individual sources: biomass burning in South America (red), Southern Africa (green), Northern Africa (blue) and Indonesia (orange), the biogenic source from isoprene (purple), methane (black, adjusted by 10 ppb) and the anthropogenic source from fossil fuel (pink) combustion for GEOS-4 at ~70 hPa.

ACPD
12, 17397–17442, 2012